The star formation history of the Sextans dwarf spheroidal galaxy: a true fossil of the pre-reionization era

M. Bettinelli,[1,2,3]★ S. L. Hidalgo,[1,2]★ S. Cassisi,[4,1]★ A. Aparicio[1,2] and G. Piotto[3,5]

[1]*Instituto de Astrofisica de Canarias, Vìa Làctea S/N, E-38200 La Laguna, Tenerife, Spain*
[2]*Department of Astrophysics, University of La Laguna, E-38200 La Laguna, Tenerife, Canary Islands, Spain*
[3]*Dipartimento di Fisica e Astronomia 'Galileo Galilei', Università degli Studi di Padova, Vicolo dell'Osservatorio 3, I-35122 Padova, Italy*
[4]*INAF-Osservatorio Astronomico d'Abruzzo, Via M. Maggini, sn. I-64100 Teramo, Italy*
[5]*INAF-Osservatorio Astronomico di Padova, Vicolo dell'Osservatorio 5, I-35122 Padova, Italy*

ABSTRACT

We present the star formation history (SFH) of the Sextans dwarf spheroidal galaxy based on deep archive *B, I* photometry taken with Suprime-Cam at Subaru telescope focusing our analysis on the inner region of the galaxy, fully located within the core radius. Within the errors of our SFH, we have not detected any metallicity gradient along the considered radial distance interval. As a main result of this work, we can state that the Sextans dwarf spheroidal stopped forming stars less than ∼1.3 Gyr after big bang in correspondence to the end of the reionization epoch. We have been able to constrain the duration of the main burst of star formation to ∼0.6 Gyr. From the calculation of the mechanical luminosity released from supernovae (SNe) during the brief episode of star formation, there are strong indications that SNe could have played an important role in the fate of Sextans, by removing almost completely the gas component, so preventing a prolonged star formation.

Key words: galaxies: dwarf – galaxies: individual: Sextans – Local Group – early Universe.

1 INTRODUCTION

Dwarf galaxies are the more common and diffused type of galaxies in the Universe. Precisely for this reason, their deep understanding could strongly influence the theories of galaxy formation and evolution. In the Λ cold dark matter (ΛCDM), scenario dwarf galaxies are building blocks of larger systems (Blumenthal et al. 1985; Navarro, Frenk & White 1997). Seen in this light, they are the survivors of early merging processes that led to the formation of bigger galaxies such as the Milky Way (MW). Thanks to their proximity, MW satellite galaxies, can be resolved into stars. From deep colour–magnitude diagrams (CMDs) reaching the oldest main sequence (MS) turn-off, the star formation history (SFH) can be derived displaying all the stars born during the lifetime of the system (Hidalgo & Aparicio 2016).

This work is part of a larger project aimed to analyse and constrain the early star formation activity in a sample of MW dwarf spheroidal (dSph) galaxies. The main goal is to discern whether these galaxies are true fossils of the reionization era (Ricotti & Gnedin 2005). There is evidence that these objects present a very old stellar population produced mostly in a single episode of star formation at early times (Grebel & Gallagher 2004; Weisz et al. 2014). The ultimate objective of our analysis is to find the imprints in the SFH of the physical phenomena that have determined the complete quenching of star formation, such as the global cosmic reionization or local effects like supernovae (SNe) feedback or tidal interactions. The first case analysed in the following work is the one of Sextans.

The Sextans dsph was discovered relatively recently by Irwin et al. (1990) during a quasars survey. It has not been possible to detect it simply by visual inspection, as it was done for the other seven classic Sculptor-like dwarfs, due to its very low central surface brightness, estimated to be 18.2 ± 0.5 mag arcmin^{-2} (Irwin & Hatzidimitriou 1995). Since its discovery many photometric surveys have been performed in order to investigate the stellar populations properties of the system. In the first data available of Irwin et al. (1990), a red horizontal branch (HB) and a well defined asymptotic giant branch were already clearly present. Mateo et al. (1991) data showed the MS turn-off, a defined red giant branch (RGB) and the presence of blue stragglers (BS). In the analysis performed by Bellazzini, Ferraro & Pancino (2001) (see also Pancino, Bellazzini & Ferraro 2002) the authors discovered the bimodal distribution in colour of the RGB stars and a double RGB-bump, unequivocally sign of two distinct stellar components, a main one with [Fe/H] ∼ −1.8 and a minor one with [Fe/H] ∼ −2.5. Lee et al. (2003) presented deep wide-field BVI photometry obtained

★ E-mail: mbettine@iac.es, marghebettinelli@gmail.com (MB); shidalgo@iac.es (SLH); cassisi@oa-abruzzo.inaf.it (SC)

Table 1. Sextans parameters.

Quantity	Value	References[a]
RA, α (J2000.0)	$10^{\rm h}13^{\rm m}03^{\rm s}.0$	(1)
Dec., δ (J2000.0)	$-1°\,36'\,52.0''$	(1)
Galactic longitude, l (°)	243.5	(1)
Galactic latitude, b (°)	42.3	(1)
Galactocentric distance (kpc)	86 ± 5	(2)
Heliocentric velocity (km s^{-1})	224.4 ± 1.6	(3)
Ellipticity, e	0.29 ± 0.03	(4)
Position angle (°)	56.7 ± 2.8	(4)
Core radius (′)	26.8 ± 1.2	(4)
Tidal radius (′)	83.2 ± 7.1	(4)
Luminosity, L_V (L$_{\odot}$)	$(4.1 \pm 1.9) \times 10^5$	(5)
Absolute magnitude, M_V	-9.2 ± 0.5	(5)
Total mass, (M$_{\odot}$)	$(4.0 \pm 0.6) \times 10^7$	(6)
Mass to light ratio, M$_{\odot}$/L$_{\odot}$	91 ± 49	(6)

References: [a](1) Irwin et al. (1990); (2) Mateo (1998); (3) Hargreaves et al. (1994); (4) Roderick et al. (2016); (5) Irwin & Hatzidimitriou (1995); and (6) Łokas (2009).

at the 3.6 m Canada–France–Hawaii Telescope (CFHT); later, Lee et al. (2009) derived the SFH making use of VI photometry. Interestingly, they found, as Pancino et al. (2002), that in the central regions the metallicity increases up to [Fe/H] ~ -1.6, while in the more external part of the investigated field metallicity decreases down to [Fe/H] ~ -1.8. The spectroscopic determinations presented in literature are systematically more metal poor: Kirby et al. (2011) measured a median [Fe/H] $= -2.00$. Lee et al. (2003) measured a similar value making use of the $(V - I)$ colour relation defined in Lee (1993), finding a mean metallicity of the RGB of [Fe/H] $\sim -2.1 \pm 0.1$, which would agree with the correlation between [Fe/H] versus M_V followed by other dwarf galaxies (e.g. Grebel, Gallagher & Harbeck 2003; McConnachie 2012).

From the structural point of view, Roderick et al. (2016) published an extensive photometric study up to 83 arcmin from Sextans' centre. The authors do not find any trace of tidal disruption but have been able to detect some overdensities equally distributed around the centre. Okamoto et al. (2017) detected the existence of an age gradient with younger stars more centrally concetrated than older ones, thus suggesting that it is unlikely that the inner region of Sextans could have been perturbed by strong tidal disruption.

The most relevant physical parameters of Sextans are summarized in Table 1.

In this paper, we present the analysis of the SFH of the Sextans dsph based on deep wide-field, ground-based photometry. The paper is organized as follows: in Section 2, the observations, data reduction, the derivation of the photometry and the photometric calibration are presented. In Section 3, the CMD of Sextans is presented. In Section 4 presents the procedure of the SFH derivation; in Section 5, it is confined the first event of star formation. In Section 5.1, we performed a radial study of the SFH. In Section 6 presents a discussion about the achieved results. Finally, in Section 7, there are the summary and conclusions.

2 OBSERVATIONS AND DATA REDUCTION

The deep wide-field photometry we present in this work is a stack of many archive observations in B and I filters, (see Table 2 for details), covering approximately an area of 34×27 arcmin centred on the galaxy, taken with the Subaru Prime Focus Camera, Suprime-Cam (Miyazaki et al. 2002) in years 2003 and 2005. We

Table 2. Observations.

Filter	ut	PI	Exposure(s)	FWHM (arcsec)
B	2005/05/04	Kleyna J.T.	500×5	0.6
B	2005/05/04	Kleyna J.T.	60×5	0.7
I	2005/02/07	Arimoto N.	270×7	1.0
I	2003/04/01	Yasuda N.	30×5	1.0
I	2003/04/03	Ikuta C.	240×5	0.6
I	2005/05/04	Kleyna J.T.	200×15	0.6
I	2005/05/04	Kleyna J.T.	60×5	0.6
I	2005/12/31	Arimoto N.	235×10	0.9
I	2005/12/31	Arimoto N.	30×3	0.9

Table 3. Parameters used for calibrating the photometry with the associated errors.

Parameter	Values
z_b	27.023 ± 0.005
c_b	0.064 ± 0.002
z_i	26.865 ± 0.014
c_i	0.056 ± 0.007

have selected the data making use of the Subaru–Mitaka–Okayama–Kiso Archive System (SMOKA) (Baba et al. 2002). Reduction, that means overscan, bias substraction, flat fielding, distortion and atmospheric dispersion corrections (see Miyazaki et al. 2002), and sky substraction, was performed using the sdfred1 software (Yagi et al. 2002; Ouchi et al. 2004). The total exposure time is 2800 s in B filter and 8936 s in I filter. The pixel scale is equal to 0.2 arcsec pixel^{-1}.

The photometry on stacked images was performed making use of the daophot/allstar suite of programs (Stetson, Davis & Crabtree 1990). We used a Moffatian of parameter $\beta = 1.5$ and radius of $R_{\rm PSF} = 15$ pixels as point spread function (PSF). From the output of allstar, only objects with $\sigma \leq 0.2$ and $-0.5 \leq$ SHARP ≤ 0.5, were taken into consideration, in order to clean up bad measured stars and galaxies. Once obtained the two catalogues in B and I filters, we performed the match using the package daomaster (Stetson 1993). From this match, the final total catalogue in B and I filters counts $\sim$86 000 stars. The data have been calibrated making use of Stetson photometric standard field for Sextans (Stetson 2000; Stetson 2005), centred on the galaxy, with an extension of 36.1×36.0 arcmin. We calibrated the entire photometric catalogue derived from the stacked images, applying the following system of two equations:

$$B - b = c_b \times (B - I) + z_b$$
$$I - i = c_i \times (B - I) + z_i, \tag{1}$$

where B, I are the standard magnitudes, b, i the instrumental magnitudes, c_b, c_i the colour therms, and z_b, z_i, the photometric zeropoints. All the coefficients relative to the two derived photometric transformations, with the corresponding errors, are listed in Table 3.

3 THE COLOUR–MAGNITUDE DIAGRAM

The CMD derived from our photometry is extended well below the oldest MS turn-off, for about 3 mag. This means that we are able to extract information till the very early epochs of Sextans and to constrain its first star formation episode. Fig. 1 shows the obtained CMD, corrected by reddening ($A_B = 0.171$, $A_I = 0.071$, Schlegel, Finkbeiner & Davis 1998; Schlafly & Finkbeiner 2011), where we over plotted three isochrones from the BaSTI stellar evolution library (Pietrinferni et al. 2004) using a distance modulus
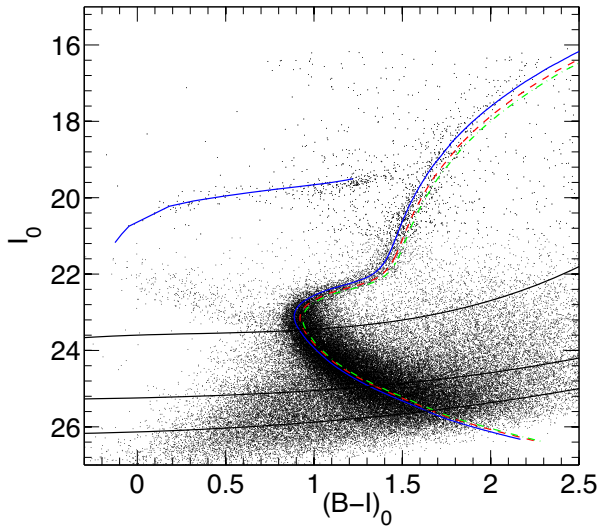
Figure 1. Observed CMD of Sextans dSph spheroidal. Three isochrones from the BaSTI stellar evolutionary library have been superimposed on the CMD: $Z = 0.0003$, 13.5 Gyr (solid blue line in the electronic version), $Z = 0.0006$, 13.5 Gyr (dash-dotted green line in the electronic version), $Z = 0.0005$, 13.5 Gyr (dashed red line in the electronic version). Red dashed line corresponds to the mean recovered metallicity for the system $[Fe/H] = -1.6$. The core helium-burning locus is given only for the $Z = 0.0003$, 13.5 Gyr isochrone (solid blue line in the electronic version). Completeness levels are over plotted as black lines: in order of increasing I_0 magnitude these are 90 per cent, 75 per cent, and 50 per cent

of $(m - M)_0 = 19.67$ (Mateo, Fischer & Krzeminski 1995). The blue and green isochrones, which correspond respectively to a metallicity of $[Fe/H] = -1.8$, $[Fe/H] = -1.5$ and an age of 13.5 Gyr, fit well the MS, the subgiant branch (SGB) and the RGB. Nevertheless, from the broadening of the RGB locus (Harbeck et al. 2001) there is some hint that there could exist a metallicity spread between $[Fe/H] = -1.8$ and -1.5. Although, one should note that this colour broadening of the RGB could be also compatible with an age spread at fixed metallicity as suggested by Okamoto et al. (2017). It is also present in the derived CMD a clear and extended blue and red HB and a quite populous region occupied by genuine BS (Okamoto et al. 2017), that means primordial binary stars that evolved in mass-transfer BS (Momany et al. 2007). The field contamination level in the central region is quite low and it has been estimated to be ∼2 per cent by Okamoto et al. (2017), so it does not significantly affect our results. Errors and completeness of the photometry are discussed in Section 4.1.

4 DERIVATION OF THE SFH

For solving the SFH of Sextans, we have followed the prescription outlined in Hidalgo, Aparicio & Gallart (2009) and Hidalgo et al. (2011). This method allows us to derive the star formation rate (SFR) as a function of time and the age–metallicity relation. The three main codes used are: (1) IAC-Star (Aparicio & Gallart 2004), that computes synthetic CMDs (sCMDs); (2) IAC-pop (Aparicio & Hidalgo 2009), the core algorithm for the calculation of the SFH solutions; and (3) MinnIAC (Hidalgo et al. 2011), a suite of routines that manages the process of sampling the parameter space, creating input data and averaging solutions. We define the SFH as a distribution function $\psi(t, z)dtdz$, which is the usual SFR but with the dependence both on time and metallicity.

4.1 The case of Sextans

First, making use of the code IAC-star (Aparicio & Gallart 2004) and the BaSTI (Pietrinferni et al. 2004) stellar evolutionary library, we computed a sCMD to be used for the analysis of the Sextans stellar properties, with 5×10^6 stars, characterized by a constant SFR between 0 and 13.5 Gyr and an uniform distribution of metallicity of $0.0001 \leq Z \leq 0.002$ for all ages. This metallicity range has been fixed accordingly to the metallicity distribution function (MDF) by Kirby et al. (2011). As bolometric corrections, we adopted Castelli & Kurucz (2004). We used as initial mass function (IMF) the one by Kroupa (2002). For the binary star distribution $\beta(f, q_{min})$, we adopted a fraction of binary stars of $f = 0.3$ and a flat distribution of the secondary to primary stellar mass ratio, q, with minimum $q_{min} = 0.5$.

As explained in deep details in (Aparicio & Gallart 1995), the simulation of observational effects is a key step for the interpretation of real data. In particular, to obtain a realistic model CMD to be compared with the real one, we need to simulate the observational effects that affect the real data. In order to estimate the completeness and uncertainties of our photometry, we followed the standard technique of injecting a list of artificial stars in each stacked image and then re-deriving the photometry in the same way as done for real stars (see Hidalgo et al. (2011)). We injected 5×10^6 stars in each image along an uniform grid, with a separation of at least $2 \times R_{PSF} + 1$ pixels between the centroids of the artificial stars. The stars have been chosen in order to cover the full range of luminosity and colour of the oCMD, $0 \leq (B - I) \leq 2.5$ and a magnitude range of $16 \leq I \leq 26$; in particular, we populated more the MS region $21.5 \leq I \leq 26$, with 3.5×10^6 stars, since it is the more relevant region for the derivation of the SFH, then the RGB region $18 \leq I \leq 21.5$, with 1×10^6 stars, and finally, the upper part of the CMD in the magnitude range of $16 \leq I \leq 18$, with 0.5×10^6 stars. In Fig. 1, we have over-plotted on the CMD of Sextans the completeness levels at 50 per cent, 75 per cent, and 90 per cent. The completeness has been calculated as the ratio of the number of artificial stars recovered to the number of all injected stars in each colour and magnitude interval. For each artificial star, we have recorded the injected magnitude m_{inj}, the recovered magnitude m_{rec}, and the position on the frame. We use the difference between the injected and recovered magnitudes ($m_{inj} - m_{rec}$) and the position of the synthetic star in the image to simulate the observational effects on the observed CMD. See Hidalgo et al. (2011) for a full description of the procedure.

In Fig. 2, we show as black dots the recovered stars with observational effects simulation and overplotted on them as red dots the observed stars. After the observational effects simulation, the distribution of stars in the oCMD is compared with the distribution of stars of each simple stellar population (SSPs) in the sCMD. The SSPs are selected by defining age and metallicity bins for the synthetic stars. For the age, we have chosen intervals of 2 Gyr for the first 8 Gyr and a finer one, of 0.5 Gyr, for the last interval between 8 and 13.5 Gyr, since it is necessary higher resolution for well characterize the first event of SFH. The metallicity bins used are: $(0.01, 0.1, 0.3, 0.5, 1, 2) \times 10^{-3}$. The higher the metallicities, the wider the intervals. Both CMDs are sampled by using *bundles*, macroregions which sample main features of the CMDs. Each of these bundles has a weight on the solution, given by the number of boxes defined in them. The larger the number of boxes, the larger the weight in the SFH.

We have defined five bundles, subdivided in boxes with varying size according to the region sampled, (see Table 4 and Fig. 2). In bundle 1, a finer grid has been used than in the other bundles, for a
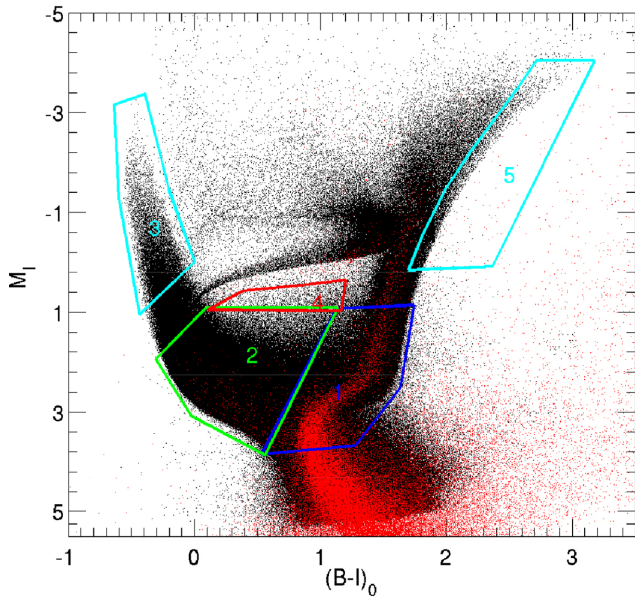
Figure 2. Synthetic CMD with the simulated observational effects (black) with overplotted the observed CMD (red). *Bundles* are the regions numbered from 1 to 5, see the text for details.

Table 4. Box sizes in each bundle that sample the observed CMD.

Bundle #	Δcol	Δmag
1	0.025	0.125
2	0.1	0.205
3	0.1	0.23
4	0.1	0.23
5	1.5	0.67

total of circa 700 boxes, since it is the region of the CMD of higher interest for the derivation of the SFH. This bundle, in fact, is the more important one for the SFH derivation because it samples the region of the CMD that is more affected by the age differences, in the sense that it corresponds to the more reliable 'clock' provided by the CMD of any stellar populations, that is the MS turn-off. Moreover, for the region of the MS stellar evolution, models are accurate and well established. Bundle 2 samples the young MS, even though in the case of Sextans these stars are recognized to be genuine BS stars (Okamoto et al. 2017). The grid has a larger binning since the density of stars is lower; in this case the boxes are about 150. Bundle 3 refers to the region of the MS occupied by the youngest stars, the so-called blue plume; in our observed CMD there are no stars in this region, but we sample it in order to constrain the resulting SFH; the boxes in this case are 20. Bundle 4 contains a portion of SGB stars (about 70 boxes) and finally, bundle 5 is an almost empty bundle with the largest box size; it constrains the maximum allowed metallicity.

In order to minimize the dependence of the solution on the CMDs sampling parameters, we obtained 24 solutions varying the CMD binning within each bundle and the SSPs sampling. To do so, we have shifted by a 30 per cent the age and metallicity in a total of 12 combinations of SSPs, each one sampled with two slightly different combinations of boxes distribution in the bundles.

To limit the effects on the solution due to uncertainties related to the distance modulus, photometric calibration, and reddening, we have shifted the oCMD 25 times along a regular grid with nodes
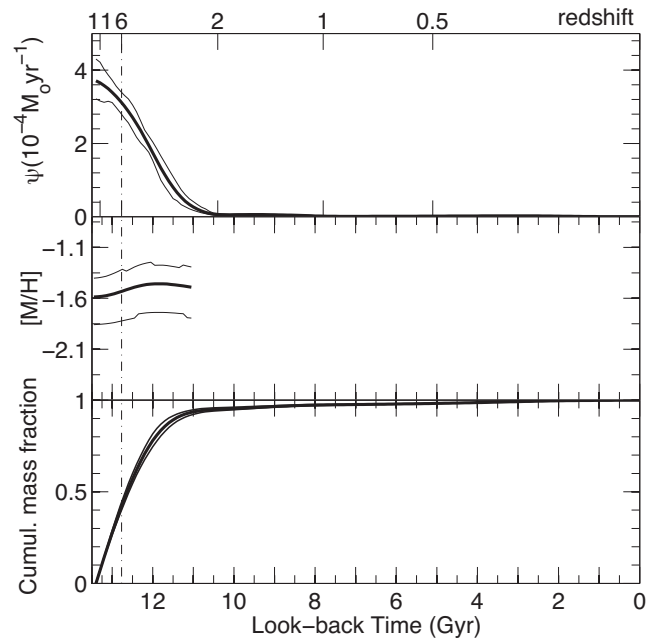

Figure 3. Results of the Sextans SFH. Top panel: SFH as a function of time ($\psi(t)$). Middle panel: metallicity of the system as a function of the time. Lower panel: cumulative mass fraction as a function of the time. Uncertainties have been drawn as this lines.

Table 5. Mass percentiles formed in Sextans as a function of redshift and look-back time.

Mass per cent	Look-back time (Gyr)	Redshift
10	13.26	10.1
20	13.11	8.3
30	12.95	7
40	12.80	6.1
50	12.64	5.4
60	12.43	4.7
70	12.22	4.15
80	11.92	3.55
90	11.45	2.9

in colour $\Delta(B - I) = [-0.1, -0.05, 0, 0.05, 0.1]$ and magnitude $\Delta I = [-0.2, -0.1, 0, 0.1, 0.2]$. For each node, we have calculated the 24 solutions described above, obtaining a total of 600 solutions. For each node, a mean solution $\overline{\psi}$ and its $\overline{\chi_\nu^2}$ is calculated. In this way, we have obtained 25 different $\overline{\chi_\nu^2}$, the one with the minimum value indicates the best solution. The best solution we have found is the one with a shift of $+0.1$ mag in I filter and no shift in colour. So that we are able to minimize the effects of the aforementioned external parameters. In Fig. 3 are plotted the obtained results. In the upper panel, it is shown the SFR as a function of time, $\psi(t)$, in the middle panel the age-metallicity relation $Z(t)$ and in the lower panel the cumulative mass function. The resolution of our results shows that Sextans has experienced a single event of star formation limited to the first ~ 2 Gyr after big bang. For clarity, we have tabulated the percentage of stellar mass produced in Table 5; it is evident that Sextans has finalized the bulk of its star formation before ~ 11.9 Gyr ago with the peak reached at ~ 13 Gyr ago. In Fig. 4, the Hess diagrams of the oCMD (left-hand panel), the best solution CMD (middle panel), and the residuals (right-hand panel) are plotted. Note here, that we have excluded foreground
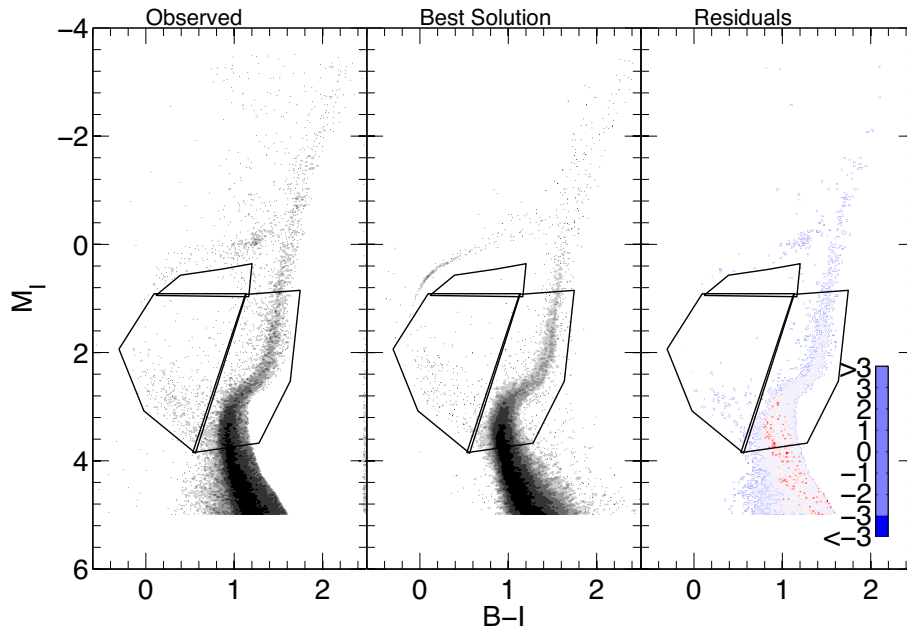
Figure 4. Hess diagrams relative to the observed CMD (left-hand panel), best solution CMD (middle panel), and residuals CMD (right-hand panel). The residuals are in units of Poisson uncertainties. Residuals from $\sigma = 0$ to $\sigma = 3$ refer to the case in which the model predicts more stars in respect to the oCMD. Residuals from $\sigma = 0$ to $\sigma = -3$ refer to the case in which the model predicts less stars in respect to the oCMD. Gray levels show the density of stars. A factor of 2 in density exists between each two successive grey levels. The single dots are shown where the density is less than 2 stars per $(0.02)^2$ mag. The boxes show the areas of the CMD used for the derivation of the SFH.

contamination points in the right-hand part of the CMD. From the residuals Hess diagram, with the values expressed in units of Poisson error, the good agreement between the observed and simulated CMD in almost all the evolutionary phases is noticeable. We note that the numerical code used for computing the synthetic CMD does not account for a dispersion of stellar masses along the core He-burning sequence as due to the occurrence of stochastic mass-loss efficiency in the previous RGB stage. This prevents the possibility to properly reproduce the colour distribution of stars along the HB in the observed CMD. Nevertheless, we wish to note that this evolutionary sequence is not accounted for in the analysis of the SFH and, hence this limitation has no impact at all on the results presented in this paper. It is interesting to note that objects at faint magnitudes to the blue side of the MS in the observed CMD are largely absent in 'best solution' CMD; these are probably unresolved faint galaxies.

## 5 CONFINING THE FIRST EVENT OF STAR FORMATION

Uncertainties deriving from observational data and from the SFH computational procedure affect the shape of the final SFH, in the sense that there is a loss of age resolution (Aparicio & Hidalgo 2009; Hidalgo et al. 2011; Aparicio et al. 2016). This effect translates into an amplification of the duration of the main event of SFH. In order to confine the duration of the first stellar burst in Sextans, we have calculated the SFH of a number of mock stellar populations with an increasing age width all starting 13.5 Gyr ago. The duration of each burst, in terms of full width at half maximum (FWHM$_{in}$), has been chosen to be: 0.25, 0.5, 0.75, 1, 1.5, 2 Gyr. Metallicity has been fixed to [Fe/H] = −1.6, which is the mean metallicity recovered for the total SFH of Sextans.

Observational effects on these mock bursts have been simulated using the completeness tests results described in Section 4.1. Then,
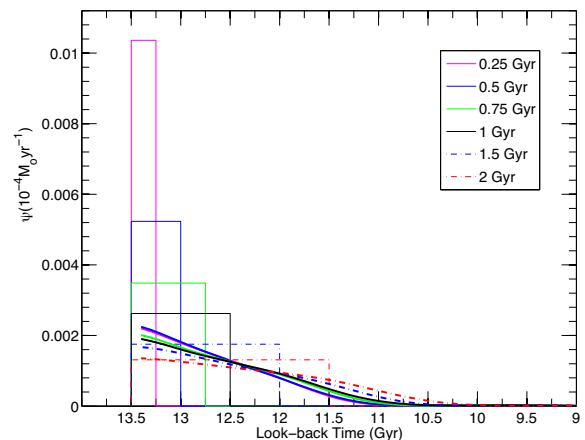
Figure 5. Recovering of an input simulated star formation burst. Input mock bursts with constant SFR and fixed time duration are shown (rectangular shape) with the recovered solution for each of them (smoothed curves).

the SFH of each mock population has been derived with the same procedure used for real data (i.e. the same *bundles* and parameters). In order to quantify the uncertainties on the recovered FWHM$_{rec}$, we have repeated five times the simulation for each synthetic burst using different random number seeds in the IAC-star input parameters. The mean recovered FWHM$_{rec}$ of each mock burst are: 2.5, 2.6, 2.8, 2.9, 3.2, 3.3 Gyr. In Fig. 5 are plotted both input mock bursts and the recovered SFHs associated with them. Since we have simulated an input constant SFR in a fixed time interval, input mock bursts have a rectangular shape, while, due to simulated photometric errors, the recovered SFHs result smoothed and broadened over a larger time interval. Fitting a Gaussian profile to the Sextans observed $\psi(t)$ in the age range 9.5–13.5 Gyr, we estimate $\sigma = 1.2$ Gyr, which corresponds to a FWHM$_{obs}$ = 2.8 Gyr.
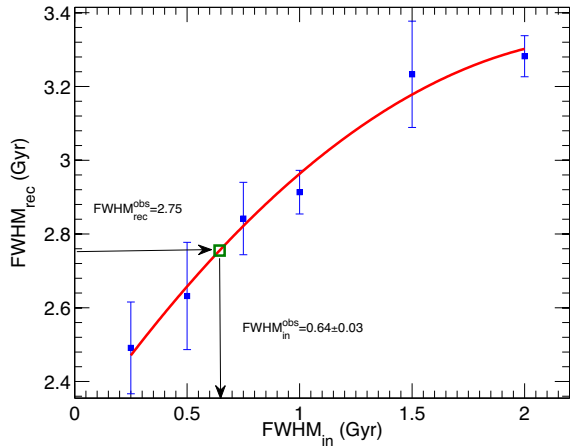
Figure 6. FWHM$_{in}$ is the FWHM of the input mock bursts, FWHM$_{rec}$, the recuperated FWHM relative to the SFH of each mock bursts. Points have been fitted with a quadratic polynomial. Knowing the FWHM of the best SFH solution, making use of the intercept on the fitting red line (see green box), we have been able to confine the first star formation burst to a value of FWHM$_{in}^{obs} \sim 0.64$ Gyr

In Fig. 6, we plotted the FWHM$_{in}$ of the mock bursts and their associated mean recovered FWHM$_{rec}$. Fitting the resulting data with a quadratic polynomial, we are able to constrain the first star formation event to an hypothetical mock burst having a FWHM$_{in} = 0.64 \pm 0.03$ Gyr. The obtained result is consistent with the estimate of about 0.8 Gyr obtained by Kirby et al. (2011) via chemical evolution models.

Seen in this light, the star formation ended close to 12.9 Gyr ago, while the end of the epoch of the reionization is fixed at $\sim$12.77 Gyr (Becker et al. 2001). This means that the star formation in Sextans was completed together to the end of the epoch of reionization.

5.1 Radial SFH

In passing, we made the attempt to investigate the radial variation of the SFH. In order to do this, we divided the area into 3 elliptical regions, with delimiting major axis of 9.65, 14.24, and 25.86 arcmin, see Fig. 7. The centre assumed for the analysis is coincident with the one tabulated by Irwin et al. (1990) in J2000.0 coordinates (153.2623, −1.6146). The position angle adopted is $\theta = 56.7$ (Roderick et al. 2016). The major axes have been fixed in order to have $\sim$29 000 stars in each elliptical region for statistical consistency. For each region, it has been derived the SFH using in each case the corresponding oCMD and as model CMD the one adopted for the total SFH. In Fig. 8 is shown the resulting metallicity as a function of time for all the 3 regions. Within errors, it is not detectable any metallicity gradient. The same can be visualized from the comparison of the cumulative mass fractions, thus indicating the absence of a radial variation of SFH. (lower panel Fig. 8).

6 DISCUSSION

The resulting SFH is globally in agreement with the findings by Lee et al. (2009) who derived the SFH from the photometry presented in Lee et al. (2003). This is also confirmed by the mean metallicity we derived, equal to [Fe/H] = −1.60 ± 0.25, which is in good agreement with the one estimated by Lee et al. (2009) in the central region of their field. Lee et al. (2009) measured that the metallicity of the stars is [Fe/H] = −1.6 in the central region, decreasing down
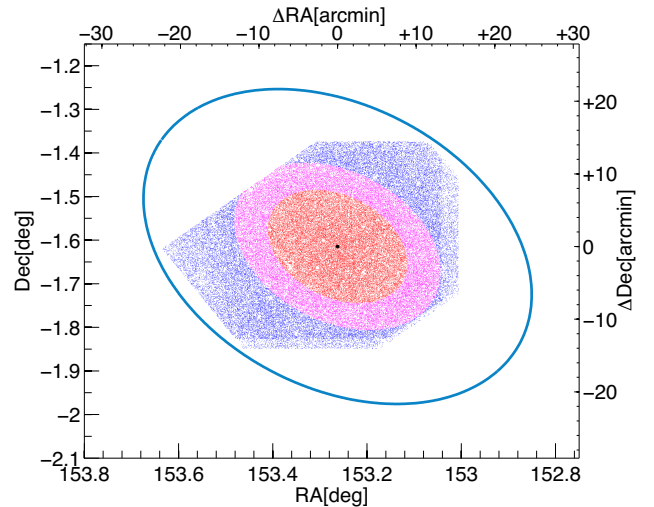

Figure 7. Stars spatial distribution, the ellipse major axis are in the intervals $a \leq 9.65$ arcmin for red points; $9.65 < a \leq 14.24$ arcmin for magenta points; and $14.24 < a \leq 25.86$ arcmin for blue points. The ellipse delimiting the core radius is plotted in light blue.
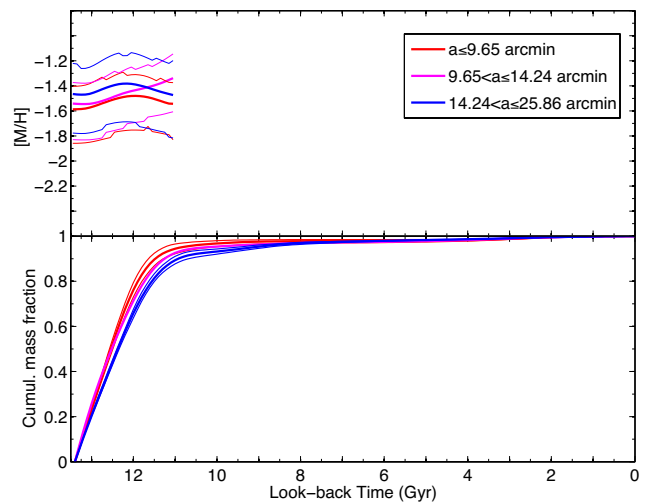

Figure 8. Upper panel: metallicity of the system as a function of the time for the three regions selected in Fig. 7. Lower panel: cumulative mass fraction as a function of the time. The same colour code as in Fig. 7 has been used. For clarity only the error bands relative to innermost and outermost regions have been shown.

to [Fe/H] = −1.8 in the outer region within the first Gyr. From our analysis, instead, emerges that metallicity in the inner core radius of Sextans does not present a radial gradient, as shown in Fig. 8, though our data span more or less the same radius of Lee et al. (2009). Moreover, the metallicity gradient measured between the innermost and the more external region in Lee et al. (2009) is of the order of $\sim$0.2 dex, a value close to the error in determination of our metallicity. This difference in the detection of the gradient could be related to a poor statistics in the number of stars used by Lee et al. (2009) for the calculation of the SFH in each region, of the order of $\sim$5000 stars, while we adopted $\sim$30 000 stars for each of our three regions. This could be also related to photometric data not deep enough, so that, the SFH is affected by large errors. In fact, in that work, the completeness for magnitude $I \sim 23.5$ is at $\sim$55 per cent, while in this work, the completeness at these magnitudes is more
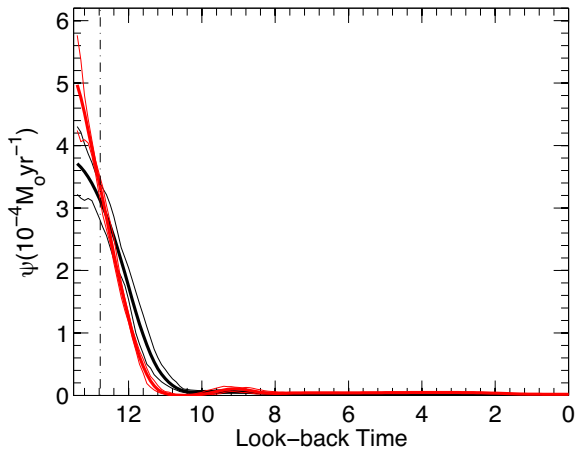
Figure 9. Original SFH, obtained without assuming any a priori MDF (in black) and the SFH derived imposing the MDF by Kirby et al. (2011) (in red).
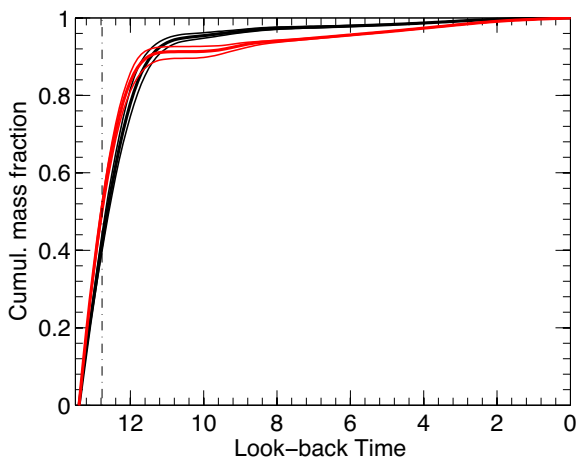
Figure 10. Cumulative mass fraction as a function of the look-back time, colour coded as in Fig. 9.

than 95 per cent. This strongly influence the result and the associated error. Another important aspect is that Lee et al. (2009) assumed that Sextans started forming stars 15 Gyr ago, while we constrained the age of the oldest acceptable population to 13.5 Gyr.

Our results on metallicity are supported by the fact that Sextans presents almost a flat [Fe/H] radial distribution from the spectroscopic measurements conducted by Kirby et al. (2011) over an area very similar to the one sampled in this work. The authors concluded that the lack of gradients, also seen in Canes Venatici I and Ursa Minor, indicates a star formation event significantly shorter than 1 Gyr. By means of chemical evolution models, they find also for Sextans, a duration of the star formation of just 0.8 Gyr, hence in striking agreement with what we found in our analysis.

But the metallicity distribution found by Kirby et al. (2011) peaks at ∼−1.8, 0.2 dex lower than our mean metallicity determination. This difference is consistent with the metallicity bin we used in the derivation of the SFH, which is ∼0.0002. As a further test, to see if the SFH is affected by this metallicity difference, we rederive it imposing an input model whose stars follow the MDF by Kirby et al. (2011). In Fig. 9 are shown the original SFH, obtained without assuming any a priori MDF (in black) and the SFH derived imposing the MDF by Kirby et al. (2011) (in red). In Fig. 10, the

cumulative mass fraction as a function of the look-back time is also shown, colour coded as in Fig. 9. The SFH in both cases is very similar in shape, demonstrating that assuming a MDF as in Kirby et al. (2011) does not change the results of this work. Moreover, assuming this MDF the star formation appears even steeper than the original one, thus confirming the trend already found without assuming any MDF for the input model. It is worth noting that even a mean metallicity of −1.6 for Sextans would be consistent with the trend in the metallicity–luminosity plane for galactic dSph (see Grebel et al. 2003; McConnachie 2012).

The question arising now is why, as detected with larger surveys, does Sextans present clear signs of the presence of a younger (and more metal rich) stellar population towards its centre, that translates in an age and metallicity gradient (see Bellazzini et al. 2001; Harbeck et al. 2001; Pancino et al. 2002; Lee et al. 2003; Rizzi et al. 2004; Okamoto et al. 2017).

Okamoto et al. (2017) through the analysis of the various evolutionary phases along a radius more extended than the tidal radius, have been able to detect an age gradient. Relatively younger stars (∼10 Gyr) are more centrally concentrated than old stars (∼13 Gyr). Through our detailed analysis, limited to the core radius, we have not detected any stellar populations gradient, so we conclude that the gradient found by Okamoto et al. (2017) has its origin after the core radius.

This point has been discussed also for the case of the isolated dSph Tucana (Monelli et al. 2010), that resemble for some aspects the case of Sextans. Tucana SFH is characterized by a unique and pronounced event of star formation and a steep rising of metallicity in correspondance of the burst followed by almost no evolution. But hints of the presence of two generations of stars have been found in the complex morphology of the HB in Tucana (Monelli et al. 2010). It is reasonable that the second generation formed towards the centre, since newly processed gas would concentrate there.

This idea is supported by the evidences found in the MDF by Kirby et al. (2011). This presents, in fact, a small bump at [Fe/H] ∼ −3, so at extremely low metallicities. This bump is interpreted by the authors as the sign of a rapid burst happened at early times followed by an epoch of minimal star formation, maybe due to SNe Type II strong ejecta.

Battaglia et al. (2011) found that within 0°.8 from the centre of Sextans, there is an high metalicity spread, with −3.8 < [Fe/H] < −1.4 and an average [Fe/H] ∼ −1.9, so partially in agreement with our results, even though our mean metallicity is ∼0.3 dex higher. In the outer region, (R > 0°.8), the metal poor population is predominant. Evidently, these stars underwent a very quick formation, while the stars in the inner part a more prolonged one.

This picture would suggest a first brief event of star formation, which produced the diffuse large-scale metal poor population and a more extended star formation that generated the centrally concentred metal rich population. From the study performed by Hidalgo et al. (2013) on the radial variation of SFH of dwarf galaxies emerges that Sextans matches the case of a typical dSph characterized by an extended old stellar population of ∼13 Gyr at all galactocentric radii and a very small age gradient towards the centre.

In the works by Ricotti & Gnedin (2005) and Bovill & Ricotti (2011), it is resumed a very stimulating aspect: the early and single star formation burst of Sextans could be an array of short bursts that we are not able to resolve with the actual techniques. The authors conclude that the metal spread and abundances, typical of dSph of the MW, are not necessarily produced by a prolonged and continuous star formation of more than 2–4 Gyr (see e.g. Grebel &

Gallagher (2004)); similar values can be obtained in the regime of bursty and multiple events of star formation with time-scales down to 50 Myr (Matteucci & Recchi 2001). This is strictly connected to the iron enrichment by SNe Ia that is uncertain and dependant on the mode of star formation. Matteucci & Recchi (2001) estimated that this time-scale varies from 40 to 50 Myr for an instantaneous starburst to 0.3 Gyr for a typical elliptical galaxy, thus far from our time resolution.

Sextans stopped early to form stars and it is of great interest to investigate if this phenomenon is linked in any way to the ultraviolet (UV) cosmic reionization, or if it is mainly due to local causes, such as intense galactic winds and SNe feedback (Lanfranchi & Matteucci 2004; Hidalgo et al. 2011; Aparicio et al. 2016).

When considering the results of the retrieved SFH as well as data in literature, the question arising is whether Sextans is 'true fossil' of the pre-reionization era in the sense introduced in Ricotti & Gnedin (2005): a dwarf that has experienced more than the 70 per cent of its star formation before the end of the reionization and that has a luminosity $L_V < 10^6 \, \mathrm{L_\odot}$. Sextans satisfies the second condition, since it has a luminosity $L_V = (4.1 \pm 1.9) \times 10^5 \, \mathrm{L_\odot}$ (Irwin & Hatzidimitriou 1995). Regarding the first condition, the galaxy formed 70 per cent of its stellar mass ~12 Gyr ago as derived from the SFH, but, as discussed in Section 5, we have been able to confine the initial event of star formation to ~0.6 Gyr, so, the above mass fraction would be completed surely within the reionization epoch.

From these two facts Sextans can really be classified a *true fossil* of the pre-reionization era. Moreover, the work by Ricotti & Gnedin (2005) corroborates the hypothesis according to which internal feedback, such as photoheating by the stars inside the galaxy and SNe explosions, have been the principal causes of suppression of star formation, since true fossils are the result of feedback processes in action prior to reionization. So that, they are expected to evolve passively after the end of the reionization era because of the exhaustion of gas; this is what the results of our analysis of Sextans are suggesting.

In order to investigate this hypothesis, we have calculated, as outlined in Hidalgo et al. (2011), the mechanical luminosity of the SNe released during the main star formation episode. This quantity together with the value of the mass of gas of the galaxy can be compared with the results presented in Mac Low & Ferrara (1999) to discern the modality according to which Sextans had lost mass in the past. Using the results from the SFH, we have calculated that a total of $9.2 \times 10^5 \, \mathrm{M_\odot}$ of gas were converted into stars. We have derived this value by scaling the SFH obtained from our observations to the whole galaxy using the King profile as obtained in Roderick et al. (2016). We obtained a total of 1.6×10^4 SNe assuming a minimum progenitor mass for core collapse SNe of $6.5 \, \mathrm{M_\odot}$ (Salaris & Cassisi 2005), and 8.7×10^3 SNe in the case of a progenitor of $10 \, \mathrm{M_\odot}$. Assuming an energy release per SN of 10^{51} erg (Leitherer et al. 1999) and a duration of the episode of 0.6 Gyr, we have calculated a total mechanical luminosity released during the old episode of $L_w = 8.2 \times 10^{38} \, \mathrm{erg \, s^{-1}}$ and $L_w = 4.6 \times 10^{38} \, \mathrm{erg \, s^{-1}}$, respectively for 6.5 and $10 \, \mathrm{M_\odot}$. From the comparison of the above values with the model results of Mac Low & Ferrara (1999) shown in their Fig. 1, it is clear that Sextans places in the region of blow-away regime in concomitance to the blow-out/mass loss regime. This result indicates that effectively SNe could have played an important role in the fate of Sextans by removing almost completely the gas component, so preventing a star formation extended over time (Dekel & Silk 1986; Kawata 2001; Chiosi & Carraro 2002). From our analysis, we cannot quantify how much reionization has

influenced the SFH of Sextans dSph, even though it has persisted during all the early evolution of the galaxy. From the simulations of Sawala et al. (2010), it is not expected that Sextans could be able to form stars after the epoch of reionization due to its relatively low mass. Moreover, there are also external effects such as the ram pressure stripping (Gatto et al. 2013) that have to be taken into account. Concerning the fact that Sextans' SFH could have been influenced by tidal interactions, from structural studies such as the one by Roderick et al. (2016) there are no clear signs of an undergoing tidal disruption from the MW.

7 SUMMARY AND CONCLUSIONS

We derived the SFH of the Sextans dsph galaxy based on deep archive *B*, *I* photometry taken with Suprime-Cam at Subaru telescope. The data are limited to the core radius of the galaxy. We have not detected any metallicity gradient along the considered radial distance interval within the errors of our SFH. We have been able to constrain the duration of the main burst of star formation to ~0.6 Gyr, thus indicating that the Sextans dsph stopped forming stars ~12.9 Gyr ago before the end of the reionization epoch. From our analysis based on the model results by Mac Low & Ferrara (1999) and the calculation of the mechanical luminosity released from SNe during the brief episode of star formation, we can advance the hypothesis that Sextans run out most of its gas reservoirs before the end of the reionization due to gas outflows induced by SNe of Type II, capable to throw out of the dwarf potential well the newly produced enriched elements and the remaining gas.

REFERENCES

Aparicio A., Gallart C., 1995, AJ, 110, 2105
Aparicio A., Gallart C., 2004, AJ, 128, 1465
Aparicio A., Hidalgo S. L., 2009, AJ, 138, 558
Aparicio A. et al., 2016, ApJ, 823, 9
Baba H. et al., 2002, in Bohlender D. A., Durand D., Handley T. H., eds, ASP Conf. Ser. Vol. 281, Astronomical Data Analysis Software and Systems XI. Astron. Soc. Pac., San Francisco, p. 298
Battaglia G., Tolstoy E., Helmi A., Irwin M., Parisi P., Hill V., Jablonka P., 2011, MNRAS, 411, 1013
Becker R. H. et al., 2001, AJ, 122, 2850
Bellazzini M., Ferraro F. R., Pancino E., 2001, MNRAS, 327, L15
Blumenthal G. R., Faber S. M., Primack J. R., Rees M. J., 1985, Nature, 313, 72
Bouwens R. J. et al., 2012, ApJ, 752, L5
Bovill M. S., Ricotti M., 2011, ApJ, 741, 18

Castelli F., Kurucz R. L., 2004, preprint (arXiv:astro-ph/0405087)
Chiosi C., Carraro G., 2002, MNRAS, 335, 335
Dekel A., Silk J., 1986, ApJ, 303, 39
Gatto A., Fraternali F., Read J. I., Marinacci F., Lux H., Walch S., 2013, MNRAS, 433, 2749
Grebel E. K., Gallagher J. S., III, Harbeck D., 2003, AJ, 125, 1926
Grebel E. K., Gallagher J. S., III, 2004, ApJ, 610, L89
Harbeck D. et al., 2001, AJ, 122, 3092
Hargreaves J. C., Gilmore G., Irwin M. J., Carter D., 1994, MNRAS, 269, 957
Hidalgo S., Aparicio A., 2016, Mem. Soc. Astron. Italiana, 87, 350
Hidalgo S. L., Aparicio A., Gallart C., 2009, The Ages of Stars, 258, 245
Hidalgo S. L. et al., 2011, ApJ, 730, 14
Hidalgo S. L. et al., 2013, ApJ, 778, 103
Irwin M., Hatzidimitriou D., 1995, MNRAS, 277, 1354
Irwin M. J., Bunclark P. S., Bridgeland M. T., McMahon R. G., 1990, MNRAS, 244, 16
Kawata D., 2001, ApJ, 558, 598
Kirby E. N., Lanfranchi G. A., Simon J. D., Cohen J. G., Guhathakurta P., 2011, ApJ, 727, 78
Kirby E. N. et al., 2011, ApJ, 727, 79
Kroupa P., 2002, Science, 295, 82
Lanfranchi G. A., Matteucci F., 2004, MNRAS, 351, 1338
Lee M. G., 1993, ApJ, 408, 409
Lee M. G. et al., 2003, AJ, 126, 2840
Lee M. G., Yuk I.-S., Park H. S., Harris J., Zaritsky D., 2009, ApJ, 703, 692
Leitherer C. et al., 1999, ApJS, 123, 3
Łokas E. L., 2009, MNRAS, 394, L102
Mac Low M.-M., Ferrara A., 1999, ApJ, 513, 142
Mateo M. L., 1998, ARA&A, 36, 435
Mateo M., Nemec J., Irwin M., McMahon R., 1991, AJ, 101, 892
Mateo M., Fischer P., Krzeminski W., 1995, AJ, 110, 2166
Matteucci F., Recchi S., 2001, ApJ, 558, 351
McConnachie A. W., 2012, AJ, 144, 4
Miyazaki S. et al., 2002, PASJ, 54, 833
Momany Y. et al., 2007, A&A, 468, 973

Monelli M. et al., 2010, ApJ, 720, 1225
Monelli M. et al., 2010, ApJ, 722, 1864
Navarro J. F., Frenk C. S., White S. D. M., 1997, ApJ, 490, 493
Okamoto S. et al., 2017, MNRAS, 467, 208
Ouchi M. et al., 2004, ApJ, 611, 660
Pancino E., Bellazzini M., Ferraro F. R., 2002, in Lejeune T., Fernandes J., eds, ASP Conf. Proc. Vol. 274, Observed HR Diagrams and Stellar Evolution. Astron. Soc. Pac., San Francisco, p. 421
Pietrinferni A., Cassisi S., Salaris M., Castelli F., 2004, ApJ, 612, 168
Ricotti M., Gnedin N. Y., 2005, ApJ, 629, 259
Rizzi L., Held E. V., Bertelli G., Saviane I., 2004, Mem. Soc. Astron. Italiana, 75, 110
Roderick T. A., Jerjen H., Da Costa G. S., Mackey A. D., 2016, MNRAS, 460, 30
Salaris M., Cassisi S., 2005, in Maurizio S., Santi C., eds, Evolution of Stars and Stellar Populations. Wiley-VCH, New York, p. 400
Sawala T., Scannapieco C., Maio U., White S., 2010, MNRAS, 402, 1599
Schlafly E. F., Finkbeiner D. P., 2011, ApJ, 737, 103
Schlegel D. J., Finkbeiner D. P., Davis M., 1998, ApJ, 500, 525
Stetson P. B., 1993, in Butler C. J., Elliott I., eds, Proc. ADD# IAU Colloq. 136: Stellar Photometry – Current Techniques and Future Developments. Cambridge Univ. Press, Cambridge, p. 291
Stetson P. B., 2000, PASP, 112, 925
Stetson P. B., 2005, PASP, 117, 563
Stetson P. B., Davis L. E., Crabtree D. R., 1990, ASP Conf. Ser. 8: IN: CCDs in Astronomy, p. 289
Strigari L. E., Bullock J. S., Kaplinghat M., Simon J. D., Geha M., Willman B., Walker M. G., 2008, Nature, 454, 1096
Tolstoy E., Hill V., Tosi M., 2009, ARA&A, 47, 371
Weisz D. R. et al., 2014, ApJ, 789, 148
Yagi M. et al., 2002, AJ, 123, 66

This paper has been typeset from a TEX/LATEX file prepared by the author.